



Interannual sedimentary effluxes of alkalinity in the southern North Sea: Model results compared with summer observations

Johannes Pätsch^{a,*}, Wilfried Kühn^a, Katharina D. Six^b

^a*Institute of Oceanography, University of Hamburg, Germany*

^b*Max-Planck Institute for Meteorology, Hamburg, Germany*

Abstract

For the sediments of the central and southern North Sea different sources of alkalinity generation are quantified by a regional modelling system for the period 2000 - 2014. For this purpose a formerly global ocean sediment model coupled with a pelagic ecosystem model is adopted to shelf sea dynamics where much larger turnover rates than in the open and deep ocean occurs. To track alkalinity changes due to different nitrogen-related processes the open ocean sediment model was extended by the state variables particulate organic nitrogen (PON) and ammonium. Directly measured and from Ra isotope flux observation derived alkalinity fluxes from the sediment into the pelagic are reproduced by the model system but calcite building and calcite dissolution are underestimated. Both fluxes cancel out in terms of alkalinity generation and consumption. Other simulated processes altering alkalinity in the sediment like net sulfate reduction, denitrification, nitrification and aerobic degradation are quantified and compare well with corresponding fluxes derived from observations. Most of these fluxes exhibit a strong positive gradient from the open North Sea to the coast where large rivers drain nutrients and organic matter. Atmospheric nitrogen deposition shows also a positive gradient from the open sea towards land and supports alkalinity generation in the sediments. An additional source of spatial variability is introduced by the use of a 3D-heterogenous porosity field. Due to realistic porosity variations (0.3 - 0.5) the alkalinity fluxes vary by about 4 %. The strongest impact on interannual variations of alkalinity fluxes exhibit the temporal varying nitrogen inputs from large rivers directly governing the nitrate concentrations in the coastal bottom water, thus, provide nitrate necessary for benthic denitrification. Over the time investigated the alkalinity effluxes decrease due to the decrease of the nitrogen supply by the rivers.

1. Introduction

- Alkalinity generation from anaerobic degradation in coastal sediments favors the marine uptake capacity for atmospheric CO₂. This is because these paths of organic matter degradation include

*Corresponding author

Email address: johannes.paetsch@uni-hamburg.de (Johannes Pätsch)



4 irreversible processes like N_2 production and loss of reduced sulfate products.
5 In September 2011 and June 2012 Brenner et al. (2016) measured alkalinity fluxes from the North
6 Sea sediment using several sediment cores. For the southern North Sea they found a mean flux
7 of $6.3 \text{ mmol m}^{-2} \text{ d}^{-1}$. Alkalinity effluxes into the pelagic system could partly determine the rel-
8 ative high surface alkalinity concentrations (Fig. 1a) in the southern North Sea as observed by
9 Thomas et al. (2009) in September 2001. Together with observed concentrations of dissolved inor-
10 ganic carbon (DIC) (Bozec et al., 2006) these surface alkalinity concentrations can be translated
11 into ΔpCO_2 values ($pCO_2^{ocean} - pCO_2^{atmosphere}$) which are mainly responsible for the air sea ex-
12 change of CO_2 between ocean and atmosphere (Fig. 1b). In the southern North Sea positive
13 values indicate oversaturation and thus outgassing, whereas in the northern parts negative values
14 result in an uptake of atmospheric CO_2 . When in a simple gedankenexperiment the observed
15 alkalinity fluxes by Brenner et al. (2016) would be reduced by 50 % from the beginning of the
16 year, the alkalinity concentrations especially in the shallow southern North Sea would be reduced
17 (Fig. 1c) and the corresponding ΔpCO_2 values would exhibit much stronger oversaturation (Fig.
18 1d). This simple experiment ignores the seasonality of the alkalinity fluxes and the fact that DIC
19 fluxes would vary in concert.
20 In this paper we investigate the variability of alkalinity generation and the efflux to the pelagic
21 zone by means of a regional biogeochemical model. The second chapter presents methods concern-
22 ing the model setup, particular with regard to the adaptation of the former open ocean sediment
23 model (Heinze et al., 1999) to shelf sea conditions. Within the third chapter model results are
24 compared with observational data. In the fourth chapter we show the results of several scenarios
25 demonstrating the sensitivity of the total model dynamics on environmental settings due to chang-
26 ing alkalinity fluxes. One of these scenarios picks up the gedankenexperiment mentioned above.
27 It demonstrates the strong impact of reduced alkalinity fluxes on the pCO_2 (see Chapter 4.2).

28 2. Methods

29 The simulations were performed with the ecosystem model ECOHAM (Pätsch and Kühn, 2008)
30 using the nesting method focussing on the central and southern North Sea (50.88° to $57.28^\circ N$,
31 $3.42^\circ W$ to $9.25^\circ E$) (Pätsch et al., 2010). The model system includes the hydrodynamic model
32 HAMSOM (Backhaus, 1985; Pohlmann, 1996; Pätsch et al., 2017) and the vertically resolved sed-
33 iment model originally developed for the deep open ocean (Heinze et al., 1999). The latter model
34 has been adopted to shelf sea dynamics, details are discussed below. The 3D fields of temperature
35 (T), salinity (S), advective flow and vertical turbulent mixing coefficients calculated by HAMSOM
36 are used as forcing for ECOHAM. The time step of ECOHAM is 5 minutes.



37 *2.1. The hydrodynamic Model*

38 The 3D fields of temperature, salinity, advective flow and vertical turbulent mixing coefficients
39 calculated by the hydrodynamic model HAMSOM are used as forcing for the pelagic biogeo-
40 chemical model ECOHAM. HAMSOM is a baroclinic, primitive equation model using the hy-
41 drostatic and Boussinesq approximations. The current velocities are calculated using a first or-
42 der component-upstream scheme. The horizontal is discretized on a staggered Arakawa C-grid
43 (Arakawa and Lamb, 1977) with a resolution of $\Delta\lambda = 1/3^\circ$ and $\Delta\phi = 1/5^\circ$.

44 In a first step the model was applied on a larger area including the Northwest European Shelf
45 ($15.250^\circ\text{W} - 14.083^\circ\text{E}$, $47.583^\circ\text{N} - 63.983^\circ\text{N}$) (Lorkowski et al., 2012). For this large-domain run
46 sea surface elevations of the semi-diurnal lunar tide M2 were prescribed at the open boundaries
47 (Backhaus, 1985). The corresponding results of temperature, salinity and surface elevation were
48 stored on the boundaries of the smaller model domain used in this study (black lines in Fig.
49 2). These data were used as boundary conditions for the hydrodynamic model HAMSOM imple-
50 mented on the smaller domain with a vertical resolution of 5 m in the upper 50 m and increasing
51 resolution below. The M2-tide is thus induced implicitly by the prescribed surface elevation at
52 the boundaries. Details of the nesting procedure can be found in Schwichtenberg (2013).

53 *2.2. The pelagic biogeochemical Module*

54 In the same way as for the hydrodynamic model in a first step the biogeochemical model ran
55 on the larger model domain and provided boundary conditions for the model on the smaller grid
56 (Fig. 2).

57 The pelagic biogeochemical model includes 4 nutrients (nitrate, ammonium, phosphate, silicate),
58 two phytoplankton groups (diatoms and flagellates), two zooplankton groups (micro- and meso-
59 zooplankton), bacteria, two fractions of detritus (fast and slowly sinking), labile dissolved organic
60 matter, semi-labile organic carbon, oxygen, calcite, dissolved inorganic carbon, and total alkalinity.
61 Calcite formation is performed by flagellates, only. The molar ratio of soft tissue production to
62 calcite production is 10:1. The model differentiates between normal exudation by phytoplankton,
63 the result of which is labile dissolved organic matter with Redfield composition corresponding
64 to the Redfield production, and an excess exudation of semi-labile organic carbon. The pelagic
65 module is described in detail in Lorkowski et al. (2012). For this study we included the prognostic
66 alkalinity calculation from Schwichtenberg (2013). The different processes (Fi) and their influence
67 on alkalinity are:

- 68 • F01 - calcite dissolution
- 69 • F02 - calcite formation
- 70 • F03 - nitrification



- 71 • F04 - uptake of nitrate
- 72 • F05 - release of ammonium
- 73 • F06 - uptake of ammonium
- 74 • F07 - atmospheric deposition of ammonium
- 75 • F08 - atmospheric deposition of nitrate
- 76 • F09 - uptake of phosphate
- 77 • F10 - release of phosphate

78 These fluxes determine the change of alkalinity:

$$\frac{\partial TA}{\partial t} = 2(F01 - F02 - F03) + F04 + F05 - F06 + F07 - F08 + F09 - F10 \quad (1)$$

79
80

81 Together with the dynamic sediment module which exchanges TA and DIC with the pelagic system
82 it was possible to simulate the full carbonate system prognostically.

83 2.3. The Sediment Module

84 2.3.1. The open ocean sediment model

85 The original sediment model was developed by Heinze et al. (1999) for the global ocean. This
86 model simulated accumulation, degradation and burial of particulate organic and shell material
87 and a diffusive pore water exchange with the overlaying ocean. It was applied mainly for the
88 deep ocean with its low amounts of incoming particulate matter compared to the shallow shelf sea
89 export. The corresponding time scales of flux variations were rather large (annual to decadal) and
90 showed no seasonal signal. This model included the solid components particulate organic matter
91 (POM), calcite, opal and silt exported from the pelagic and the dissolved components phosphate
92 (PO_4), dissolved inorganic carbon (DIC), alkalinity (TA), silicate ($\text{Si}(\text{OH})_4$), nitrate (NO_3), oxy-
93 gen (O_2), and dinitrogen (N_2).
94

95 2.3.2. The vertical resolution

96 The upper 156 mm of the sediment are resolved by 12 layers with increasing thickness (2 - 24
97 mm). Below the deepest layer a dimensionless burial layer is implemented.
98



99 *2.3.3. New Components*

100 As the pelagic model delivers sinking particulate material with freely varying stoichiometry, we
 101 differentiated benthic POM into the state variables particulate organic carbon (POC), nitrogen
 102 (PON) and phosphorus (POP). Additionally we added ammonium (NH₄) as product of the in-
 103 complete aerobic degradation which can be oxidised by nitrification when oxygen is available
 104 (Paulmier et al., 2009). Nitrite is not explicitly included. The model combines the effect of sul-
 105 fate reduction and reoxidation of reduced sulfate compounds as net sulfate reduction (i.e., sulfate
 106 reduction minus reoxidation). The different reaction equations including the alkalinity generation
 107 are listed in the appendix.

108

109 *2.3.4. Varying Porosity*

110 The effectivity of several sediment reactions depends on the porosity, i.e., the portion of pore water
 111 in a given sediment volume. While the global coarse grid sediment model was implemented with
 112 a horizontally uniform porosity (Heinze et al., 1999), in the presented shelf application varying
 113 porosities were taken into account. The main parts of the North Sea sediments consist of sand,
 114 but there are also muddy areas and even rocky areas exist. The different sediment classes are
 115 defined by the composition of grains with different diameters. W. Puls kindly delivered us a
 116 North Sea wide map of such grain compositions (pers. comm.). As the sediment model uses
 117 porosity values (P), the different grain size distributions have to be mapped to porosity values.
 118 We used the median grain size ($D50$) to calculate the porosity (pers. comm. W. Puls):

$$P_{surf} = \min(1, \max(0.3, 0.2603 \cdot 1.20325^{D50})) \quad (2)$$

$$D50 = -\log_2 d \quad (3)$$

119 where d is the grain diameter in mm.

120 The resulting porosity values P_{surf} fall in the range [0.3,1]. Only for rocky sediments the porosity
 121 is defined as zero (Fig. 2). According to Heinze et al. (1999) porosities $P(z)$ in deeper layers were
 122 defined in relation to the top layer:

$$P(z) = P_{surf} \cdot e^{k_0 \cdot z(m)} \quad (4)$$

123 For $k_0 = 2.12$ and $P_{surf} = 0.3$ the deepest layer at $z_{k=12} = -0.144$ m obtains a value of $P(z_{k=12}) =$
 124 0.22.



Process	Turnover Rates	Open Ocean	Shelf	unit	Eqn. No
aerobic degradation	r1	$1.160 \cdot 10^{-13}$	$2.000 \cdot 10^{-10}$	$\frac{m^3}{mmol O_2 \cdot s}$	(7)
denitrification	r2	$1.157 \cdot 10^{-7}$	$1.736 \cdot 10^{-3}$	$\frac{1}{s}$	(8)
sulfate reduction	r3	$1.157 \cdot 10^{-9}$	$3.472 \cdot 10^{-9}$	$\frac{1}{s}$	(9)
calcite dissolution	r4	$1.000 \cdot 10^{-13}$	$1.000 \cdot 10^{-8}$	$\frac{m^3}{mmol CO_3^{2-} \cdot s}$	(10)
opal dissolution	r5	$1.000 \cdot 10^{-12}$	$1.000 \cdot 10^{-11}$	$\frac{m^3}{mmol SiO_2 \cdot s}$	(11)
nitrification	r6		$1.157 \cdot 10^{-4}$	$\frac{1}{s}$	(12)

Table 1: Comparison of open ocean (Heinze et al., 1999) and shelf (this study) turnover rates.

125 2.3.5. Turnover Rates

126 The reaction equations and the chosen stoichiometries are described in detail in the Appendix.

127 These equations use turnover rates which were modified in comparison to the original open ocean

128 sediment model (see Table 1)

129 2.3.6. Temperature Dependency

130 As the shallow water column in the North Sea exhibits strong seasonal temperature variations

131 ($\Delta T > 15^\circ C$) a temperature dependency of both, the turnover rates (see Appendix) and the

132 vertical diffusion was implemented.

133 A Q_{10} value of 1.2 for aerobic degradation, denitrification, nitrification, sulfate reduction and the

134 dissolution of calcite and opal was chosen (see Appendix).

135 The vertical diffusion coefficient for all pore water tracers in the original open ocean model was

136 constant ($d_v = 10^{-9} \frac{m^2}{s}$). In the shelf model the coefficients were defined as temperature (T) and

137 porosity (P) dependent (Gypens et al., 2008):

$$d_v = \begin{cases} (d_0 + a \cdot T) \cdot P & : P < 0.4 \\ (d_0 + a \cdot T) \cdot P^2 & : P \geq 0.4 \end{cases}$$

138 The parameters d_0 and a are defined in Gypens et al. (2008) (their Table 2) for different groups of

139 pore water tracers: The lowest coefficient is defined for phosphate ($d_{v_{pho}}(T_{10}) = 5.4 \cdot P \cdot 10^{-10} \frac{m^2}{s}$)

140 a medium coefficient ($d_{v_{tra}}(T_{10}) = 1.4 \cdot P \cdot 10^{-9} \frac{m^2}{s}$) is valid for the biogeochemical tracers DIC,

141 nitrate, ammonium, alkalinity and silicate. The highest coefficient was defined for the gases oxygen

142 and dinitrogen ($d_{v_{nit}}(T_{10}) = 1.6 \cdot P \cdot 10^{-9} \frac{m^2}{s}$), all at $T_{10} = 10^\circ C$ and a porosity $P < 0.4$, which

143 is typical for sandy ground. In order to take into account advective exchange of pore water with

144 the pelagic system the coefficients for the uppermost layer were increased by a factor of 10. This

145 factor was determined by several sensitivity runs to balance the exchange between the sediment

146 and the pelagic. The same factor is used by Neumann et al. (2017) to switch between diffusive and



147 advective nitrate exchange between sediment and pelagic in the German Bight. The temperature
148 of the sediment was defined as the temperature of the lowest pelagic layer.
149 The vertical diffusion coefficient for DIC compares well with the corresponding coefficient given
150 by Burdige and Komada (2013) (their Table 3) for $T = 5^{\circ}\text{C}$ and $P = 0.36$.

151

152 *2.4. External Data*

153 The meteorological forcing (Kalnay et al., 1996) and the river loads of carbon, alkalinity, nutrients
154 and organic compounds have been implemented according to Lorkowski et al. (2012). To treat
155 these tracers more realistically in this study also daily freshwater discharge of the rivers was used
156 (Pätsch et al., 2016). In this way the input of tracers from the rivers (mmol d^{-1}) can be an
157 effective source or sink depending on the concentrations of the tracers in the river water.

158 The calculated shortwave incoming radiation has been reduced by 10% as it has been shown
159 that the sea surface temperature (SST) would otherwise be overestimated (compare Fig. 3 in
160 Lorkowski et al. (2012)).

161 The atmospheric nitrogen deposition was derived following Große et al. (2016), using annual data
162 from the EMEP (Cooperative program for monitoring and evaluation of the long-range transmis-
163 sions of air pollutants in Europe) model. As our simulation period exceeds the period of data
164 available from EMEP a long-term trend according to Schöpp et al. (2003) was applied in addition.
165 Atmospheric deposition is implemented as inputs of nitrate and ammonium.

166 *2.5. The Experiments*

167 For each experiment described below the biogeochemical simulation in the central and southern
168 North Sea area spun up over 20 years repeating the year 2000 until all processes were in equilibrium
169 and did not change from year to year. After this procedure the years 2000 to 2014 were simulated
170 consecutively.

171

172 Different experiments or scenarios were performed:

- 173 • The **reference run** with the new sediment module provides a basis with realistic boundary
174 conditions and horizontally varying porosities.
- 175 • In order to reproduce a situation without anthropogenic influence, we reduced the inorganic
176 and organic river input of nitrogen and phosphorus to 10 % of the reference run. Addition-
177 ally the atmospheric deposition of nitrogen was reduced to 28 %. This run more or less
178 reproduced the "**pristine conditions**" Serna et al. (2010) established.



- 179 • To analyse the impact of the new sediment module on the pelagic system we compare the
180 results of the reference run with results of the scenario "plate run". In this scenario a simple
181 sediment module was used, which collects, remineralises and releases the sunken particulate
182 organic material on a two dimensional plate (Pätsch and Kühn, 2008).
- 183 • In the reference run horizontally varying porosities were used. To study the influence of this
184 feature we conducted two additional model runs with basin wide uniform porosities: One
185 with the minimum porosity $P_{\min} = 0.3$ found in the model domain of the reference run and
186 one with the maximum porosity $P_{\max} = 0.51$.

187 3. Comparison with Observations

188 To get confidence into the adapted sediment model we compared simulated and observed fluxes
189 between sediment and pelagic. Additionally, simulated pore water profiles were compared with
190 observed profiles.

191 3.1. Oxygen Fluxes

192 Brenner et al. (2016) measured the total oxygen consumption of sediment cores which can be
193 compared with simulated oxygen fluxes into the sediment. The corresponding available data and
194 their positions are shown in Fig. 3 (rectangles). The underlying map of simulated oxygen fluxes
195 at the time when observations were taken show reasonable values. Only in the German Bight
196 the model underestimates the measurements. An explanation for this effect is that particulate
197 organics (POM) imported by the rivers are considered as slowly sinking detritus. As consequence
198 the horizontal export of POM out of the German Bight is overestimated and the local flux into
199 the sediment is underestimated.

200 3.2. Alkalinity Fluxes

201 Fig. 4 shows the comparison of fieldwide averaged alkalinity effluxes and the contributions from
202 aerobic degradation, denitrification, net sulfate reduction, nitrification and calcite dissolution from
203 observations in September 2011 (Brenner et al., 2016) and from our model results for September
204 2011. For the observational data only the spatial standard deviation of alkalinity efflux is given
205 (see grey error bar in Fig. 4a). The temporal standard deviation of the simulated daily values
206 within September 2011 is for all fluxes very small and not shown ($< 0.003 \text{ mmol m}^{-2} \text{ d}^{-1}$). The
207 spatial standard deviation of the simulated September fluxes are shown as error bars in Fig. 4b.
208 Even though the simulated efflux lies within the high spatial variability of the observed alkalinity
209 efflux, the model rather underestimates all contributions. Only the simulated contribution from
210 aerobic degradation is larger than the corresponding observation. The main deviation can be
211 attributed to the low simulated calcite dissolution within the sediment.



212 In comparison to other models (Ridgwell et al., 2007; Lorkowski et al., 2012) the ratio of sim-
213 ulated particulate organic carbon to particulate inorganic carbon (POC:PIC) or the simulated
214 organic carbon to calcite production ($10 \text{ mol POC d}^{-1} : 1 \text{ mol calcite d}^{-1}$) is relatively low mean-
215 ing high calcite production in relation to organic carbon production. Nonetheless our model still
216 leads to an underestimation of the calcite dissolution in the sediment compared to the analysis of
217 Brenner et al. (2016). The mean simulated calcite deposition into the sediment in September 2011
218 was $2.9 \text{ mmol m}^{-2} \text{ d}^{-1}$, which is still only 54 % of the observed calcite dissolution in the sediment.

219

220 Fig. 5 shows the corresponding simulated alkalinity fluxes to the pelagic system for 15 September
221 2011. The alkalinity efflux is strongest in the German Bight near the mouth of River Elbe. The
222 flux decreases with distance from the continental coast. Elevated values can be seen off the Danish
223 coast. Similar features can be observed for the contributors aerobic degradation, denitrification,
224 net sulfate reduction, and calcite dissolution. The distribution of the negative fluxes due to
225 nitrification shows also elevated values in the German Bight.

226 When ignoring the sedimentary calcite dissolution in both the simulation and the observed data,
227 the remaining alkalinity generation compares better with the observations (Fig. 6). The colors
228 within the four rectangles identify the strength of the observational data whereas the horizontal
229 distribution shown by the colored map stands for simulations. Only in the inner German Bight the
230 simulated flux appears far too low. An explanation for this effect is the same as for oxygen fluxes:
231 The export of POM out of the German Bight is overestimated and thus local remineralization
232 underestimated.

233 3.3. Profiles

234 During the cruise He-308 in May 2009 several sediment cores in the German Exclusive Economic
235 Zone (EEZ) were taken and investigated. The nitrate data are published by Neumann et al.
236 (2017), all data are archived in Pangaea (2017). We compare our results of the reference run
237 with observed data of oxygen, nitrate, phosphate and ammonium (Fig. 7). To understand the
238 model sensitivity, also the corresponding profiles of the "pristine conditions" run are shown. The
239 position of the chosen core is between the German coast and the island Helgoland ($54^{\circ} 5' \text{ N}$, 8°
240 E). This area is strongly affected by high nutrient loads from the continental rivers and high atmo-
241 spheric nitrogen deposition (Pätsch et al., 2010) resulting in significant differences in the simulated
242 porewater concentrations of the reference run and the scenario "pristine conditions" (solid and
243 dashed black lines). The simulated oxygen penetration depth (concentration $< 10 \text{ mmol O}_2 \text{ m}^{-3}$)
244 is about 0.5 cm which fits to the observations (Fig. 7a). It is about 0.8 cm in the scenario "pris-
245 tine conditions". In the upper 0.4 cm the model underestimates in both scenarios the observed
246 oxygen concentrations. Fig. 7b shows the profiles of observed NO_x including nitrate and nitrite



247 and the profiles of simulated nitrate. We think that this is a proper comparison as observed ni-
248 trite concentrations are low ($< 0.8 \text{ mmol N m}^{-3}$, not shown). Observed NO_x concentrations are
249 detectable only in the upper 2 cm. Due to uncalibrated measurements deeper values appear dis-
250 criminable from zero concentration, but they should be interpreted as zero concentration (pers.
251 comm. Andreas Neumann). The simulated concentrations (reference run) reach very low values
252 already at 1 cm depth, the "pristine conditions" scenario shows very low concentrations already
253 at 0.5 cm depth. Observed phosphate concentrations in Fig. 7c indicate two mixing regimes: In
254 the upper 9 cm the sediment core shows concentrations slightly increasing with depth, below a
255 stronger gradient can be seen. The upper part appears well-mixed while in the lower part mixing
256 decreases. This effect might be caused by bioturbation and bioirrigation in the upper 9 cm. As the
257 latter processes are not included in the model we got a more homogenous picture of the phosphate
258 profiles. The model (reference run) overestimates the observational values in the upper part while
259 it underestimates them in the lower part. A similar pattern can be seen for ammonium (Fig. 7d),
260 where again the observational concentrations indicate an upper and a lower mixing zone. The
261 simulated values increase between the surface and the 5 cm horizon, below they are more or less
262 constant. The values of the reference run are too high in the upper 13 cm. These high simulated
263 ammonium values might be caused by neglecting the process of anammox in the model. This
264 process transforms reactive nitrogen compounds (ammonium and nitrite) into inert molecular ni-
265 trogen. Similar high ammonium concentrations can be found in Luff and Moll (2004) within their
266 Fig. 9.

267

268 4. Results

269 4.1. Temporal Variations

270 The temporal development of monthly alkalinity effluxes (2000 - 2014) without calcite dissolution
271 of a near coast station (54° N , 8° E) shows an overall decreasing trend (Fig. 8). To understand
272 this feature the sources of alkalinity generation and the annual loads of nitrate by the River Elbe
273 (Radach and Pätsch, 2007; Pätsch et al., 2016) in the German Bight (53.9° N , 8.9° E) are shown
274 (see Fig. 1a). Calcite dissolution is very variable and exhibits a decrease over the simulation
275 period. Because of its high variability which would overwrite the nitrogen-related signals calcite
276 dissolution is not shown.

277 Aerobic degradation with a distinct annual cycle appears quite constant over the years. Sulfate
278 reduction is more or less constant, while nitrification (as negative contribution) shows a positive
279 trend in opposite to the negative trend of denitrification. The dark blue line represents the nitrate
280 discharge of the nearby River Elbe. With strong seasonal peaks it exhibits a negative trend which
281 can explain a similar trend in denitrification.



282 Strong nitrate discharge events are followed some months later by local maxima in denitrification.
283 This can be seen in 2003 and 2011. Over several successional winter months in 2007/2008 high
284 nitrate loads lead to strong denitrification in 2008. In all these years the TA efflux was elevated.

285 4.2. Alkalinity Generation and pCO_2

286 As already demonstrated in the gedankenexperiment in the introduction the alkalinity release from
287 the sediment has a significant impact on the carbonate system and thus on the ΔpCO_2 regulating
288 the exchange of CO_2 between the atmosphere and the sea.

289 Using the simulated timeseries 2000 - 2014 (reference run) we analysed the cumulative alkalinity
290 efflux out of the sediment from the beginning of the year 2011 to mid September 2011 (Fig. 9a).
291 Near the Danish coast we found a flux of about 1000 mmol m^{-2} for this period. For the inner
292 German Bight even higher values can be found. These maxima result in corresponding areas of
293 strong undersaturation in respect of ΔpCO_2 on September 15 (Fig. 9b). The interior and the
294 northwestern part are slightly oversaturated.

295 Fig. 9c shows the alkalinity flux of the "pristine conditions" run until September 15. The flux
296 reduction (compare with Fig. 9a) is strongest ($\approx 20\%$) in areas where the generation of alkalinity
297 was strongest. Areas of oversaturation of ΔpCO_2 (Fig. 9d) increase and especially in the shallow
298 areas with high sediment impact the previously undersaturated situations turn into oversaturation
299 (or light undersaturation). Because of the distance to the rivers the situation is more or less
300 unchanged in the central part.

301 4.3. Sensitivity on different porosities

302 To investigate the effect of spatially varying porosities we conducted two additional simulations
303 which were spun up separately : One with a basin wide uniform porosity with the minimum value
304 of the reference run except for rocks ($P_{\min} = 0.3$) and one with the maximum value ($P_{\max} = 0.51$).
305 For the different annual fluxes between the sediment and the pelagic at $54^\circ 5'N$, $8^\circ E$ the relative
306 deviations (%) of these two runs are analysed for 2011 (Fig. 10).

307 Switching over from the P_{\min} to the P_{\max} run the diffusive flux of DIC, alkalinity and phosphate
308 out of the pore water of the sediment increases by about 4%. The flux of silicate from the
309 sediment increases by 16%. Also the import of oxygen and nitrate increase. This overall increase
310 is astonishing as the effective diffusivity decreases when the porosity passes over the limit of 0.4
311 (see section 2.3.6). Of interest are also the deviations of the five contributors to the alkalinity flux,
312 i.e., the alkalinity flux due to the aerobic degradation (+7%), the calcite dissolution (+3.4%), the
313 denitrification (+1.5%), the sulfate reduction (-7.8%) and the (negative) nitrification (-0.5%).
314 Sulfate reduction decreases as the amount of POC reaching the deeper sediment layers decreases
315 due to the enhanced aerobic remineralisation.



316 Due to positive feedback mechanisms on the nutrients in the water column the sinking fluxes of
317 particulate organic matter (POC, PON, POP) increase. The largest increase in solids entering
318 the sediment can be found for opal (+5.6 %) corresponding with the large silicate efflux from the
319 sediment into the pelagic. Calcite export slightly decreases as the silicon shell building diatoms
320 are favored by the increased silicate availability.

321 4.4. Comparison of the vertical resolved and the plate sediment module

322 In former model versions (Pätsch and Kühn, 2008; Lorkowski et al., 2012; Große et al., 2016) the
323 sediment was represented by a two-dimensional plate without depth resolution. The sinking ma-
324 terial was gathered and remineralised on the surface of this plate. The remineralisation rates had
325 been adjusted so that the particulate material from the last year was more or less dissolved and
326 released until February/March of the following year.

327 The temporal development of carbon exchange between sediment and pelagic in 2011 at $54^{\circ} 5' N$,
328 $8^{\circ} E$ is shown in Fig. 11a for the "plate run". The time in the year when half of the exported
329 particulate material is returned as DIC ("half time") is indicated by the black arrow on the x-axis.
330 For the "plate run" this is day 230.

331 Fig. 11b shows the corresponding carbon fluxes of the reference run. While the shape of the curve
332 representing the particulate export is similar to that of Fig. 11a, the remineralisation flux shows
333 less temporal variation. Due to the high remineralisation flux in winter the "half time" is reached
334 earlier (day 207).

335 5. Discussion

336 5.1. Nitrogen related processes

337 After calcite dissolution benthic denitrification is the second largest positive contribution to alka-
338 linity generation (Fig. 4). Near-bottom nitrate concentration which is correlated with near bottom
339 oxygen saturation governs the direction of nitrate exchange across the pelagic - sediment interface
340 (Neubacher et al., 2011). In case of the invasion of pelagic nitrate into the sediment benthic den-
341 itrification is stimulated. The other source of benthic nitrate is the benthic nitrification which is
342 driven by oxygen within the sediment. At $54^{\circ} N$, $8^{\circ} E$, however 86 % of oxygen are consumed by
343 aerobic degradation and only 14 % by benthic nitrification. For shelf seas Seitzinger and Giblin
344 (1996) estimated the local benthic denitrification rate (DNR) to be about 2 % of the local primary
345 production (PP). This estimate, of course, can be influenced by parameters like water depth, ad-
346 vection, and near bottom oxygen consumption. Indeed the evaluation of our reference run shows
347 that the relation $r = \text{DNR}/\text{PP}$ was about 2 % in regions with water depth of about 30 m and an
348 annual Redfield production (see 2.2)) of about $150 \text{ g C m}^{-2} \text{ yr}^{-1}$, which can be found some tens
349 of kilometers off the mouths of the big rivers. According to our simulations r is only larger than



350 2% near the mouth of River Elbe. For all other regions r ranges between 1.1% and 1.4%.

351

352 In the case of the ammonium profile (Fig. 7d) the "pristine conditions" simulation matches the
353 observation better than the reference run. This might have to do with the absence of the process
354 anammox within the model which would consume ammonium under presence of nitrite.

355

356 The comparison of the reference run and the "pristine conditions" run exhibits a deeper penetration
357 of oxygen into the sediment for the pristine more nutrient depleted scenario (Fig. 7a). This is in
358 accordance with the findings of Neubacher et al. (2011) who differentiated a realistic and a rich
359 hypoxic situation, the latter with lower penetration depths.

360 5.2. Sources of Alkalinity

361 An effective tracer of North Sea total alkalinity is the naturally occurring radium isotope ^{228}Ra
362 (Burt et al., 2014). These authors estimated a coastal alkalinity input of $3.4 - 23.6 \text{ mmol m}^{-2} \text{ d}^{-1}$
363 into the southern North Sea ($A=190.765 \text{ km}^2$) in September 2011. This input was assumed to come
364 mainly from the Wadden Sea. The amount of this input lies in the same range Brenner et al. (2016)
365 estimated as total input from the sediments into the pelagic southern North Sea (Fig. 4). This
366 estimate is valid for a late summer situation and includes the large effect of calcite dissolution. For
367 the southern North Sea calcite dissolution and production is roughly balanced on an annual basis.
368 The estimate by Burt et al. (2014) and the measurements by Brenner et al. (2016) appear high
369 in comparison to the value given by Thomas et al. (2009) who estimated an alkalinity input from
370 the Wadden Sea of $1 \text{ mmol m}^{-2} \text{ d}^{-1}$ into the south-eastern North Sea over the year. This value
371 was calculated using an alkalinity budget which does not differentiate input from autochthonous
372 sediment and from the adjacent Wadden Sea and, additionally, does not take into account calcite
373 production and dissolution.

374 Together with our simulation results the following picture can be given: The relative high flux
375 estimates by Burt et al. (2014) and Brenner et al. (2016) can be explained by the inclusion of calcite
376 dissolution and the time in the year when measurements were taken. When calcite dissolution is
377 excluded our annual estimate for the total model region ($0.4 \text{ mmol m}^{-2} \text{ d}^{-1}$) can be compared with
378 the estimate by Thomas et al. (2009) for the south-eastern North Sea with higher productivity
379 than the average of the model region.

380 6. Conclusion

381 Even though our model may slightly underestimate benthic denitrification in the southern North
382 Sea it reveals this process as the largest net contribution to alkalinity generation in this area.
383 This compares well with the estimates by Brenner et al. (2016) when the dissolution of calcite is



384 not taken into account, because the observational data might miss the calcite production signal
385 which then would cancel out the effect on alkalinity. Estimates of other alkalinity fluxes like
386 alkalinity generation in the Wadden Sea are not taken into account as their estimates appear
387 not well constrained. A direct modelling approach of such sources of alkalinity appears necessary
388 (Schwichtenberg, 2013), but is beyond the scope of this study.

389 7. Acknowledgement

390 This work was supported by the Cluster of Excellence CliSAP (EXC177), University of Hamburg,
391 funded by the German Science Foundation (DFG). We thank Ernst Maier-Reimer who can be im-
392 mediately identified as coauthor of the model code, Helmuth Thomas, Hermann Lenhart, Alberto
393 Borges, Markus Kreuz, Fabian Schwichtenberg and Fabian Große for valuable discussions.

394 8. Figure Caption

395 Fig. 1 a) Surface alkalinity concentrations (mmol kg^{-1}) measured in September 2001, b) corre-
396 sponding ΔpCO_2 (ppm), the difference of partial pressure of ocean and atmospheric pCO_2 , c)
397 reduced alkalinity concentrations due to a reduction of 50 % of the estimated alkalinity flux by
398 Brenner et al. (2016), d) ΔpCO_2 corresponding to the reduced alkalinity in c).

399
400 Fig. 2 Porosity field according to W. Puls (pers. comm.). Blue areas indicate rocky sediments, red
401 areas indicate muddy sediments with low grain diameters and green areas indicate sandy ground.
402 The black lines indicate the model boundaries.

403
404 Fig. 3 Simulated and observed oxygen fluxes ($\text{mmol O}_2 \text{ m}^{-2} \text{ d}^{-1}$) for 15 September 2011. The ob-
405 servations by Brenner et al. (2016) are indicated by the colored rectangles.

406
407 Fig. 4a): Mean observed alkalinity flux for the southern North Sea in September 2011. Addition-
408 ally the derived mean alkalinity generation due to aerobic degradation, denitrification, net sulfate
409 reduction and calcite dissolution are shown. A sink for alkalinity is nitrification. All fluxes in
410 $\text{mmol m}^{-2} \text{ d}^{-1}$ (Brenner et al., 2016). b): Simulated alkalinity flux for the southern North Sea on
411 15 September 2011. Additionally the alkalinity generation and reduction due to aerobic degrada-
412 tion, denitrification, net sulfate reduction, nitrification and calcite dissolution are shown. The grey
413 error bars indicate the spatial standard deviation.

414
415 Fig. 5 a) Simulated net alkalinity generation and corresponding sources and sinks due to b) aerobic
416 degradation, c) denitrification, d) net sulfate reduction, e) nitrification, f) calcite dissolution on



417 15 September 2011. All fluxes in $\text{mmol m}^{-2} \text{d}^{-1}$. The scale of a) - d) is identical.

418

419 Fig. 6 Simulated and observed alkalinity generation ($\text{mmol m}^{-2} \text{d}^{-1}$) without calcite dissolution
420 for 15 September 2011. The observations are indicated by the colored rectangles.

421

422 Fig. 7 Profiles of porewater concentrations of a) oxygen, b) nitrate, c) phosphate and d) ammonium
423 at $54^{\circ} 5' \text{N}$, 8°E in May 2009. Nitrate data were published by Neumann et al. (2017). The black
424 solid line indicates the reference run, the dashed black line represents the results of the "pristine
425 conditions" scenario and the different blue lines are derived from observations during the cruise
426 He-308. In the figures b-d repeated observational profiles are shown. Notice the different profile
427 depths.

428

429 Fig. 8 Simulated monthly values of alkalinity efflux from the sediment without calcite dissolu-
430 tion at 54°N , 8°E , the corresponding sources and sinks due to aerobic degradation, deni-
431 trification, net sulfate reduction, nitrification and the annual loads of nitrate from River Elbe
432 (Radach and Pätsch, 2007; Pätsch et al., 2016). Note: nitrification has a negative contribution to
433 the alkalinity generation.

434

435 Fig. 9 a) Simulated cumulative alkalinity generation in 2011 until September 15 (mmol m^{-2})
436 for the reference run b) the corresponding $\Delta p\text{CO}_2$ on September 15, c) cumulative alkalinity
437 generation until September 15 with reduced river input (10%) and only 28 % atmospheric nitrogen
438 deposition ("pristine conditions"), d) $\Delta p\text{CO}_2$ on September 15 ("pristine conditions").

439

440 Fig. 10 Deviations between the "high" and the "low" porosity run. Shown is the relative change
441 of annual fluxes (%) between the sediment and the pelagic for a station at $54^{\circ} 5' \text{N}$, 8°E in 2011.
442 DIC, TA, PO_4 , SiO_4 , N_2 , NH_4 indicate the diffusive fluxes of dissolved matter from the sediment
443 into the pelagic. Ox and NO_3 are corresponding fluxes from the pelagic into the sediment. aeralk,
444 cacalk, dnalk, suralk and nitalk indicate the partitioning of the alkalinity flux according to its
445 sources aerobic degradation, calcite dissolution, denitrification, sulfate reduction and nitrification,
446 respectively. The fluxes of solids from the pelagic into the sediment are POC, PON, POP, OPAL
447 and CaCO_3 .

448

449 Fig. 11 Temporal development of carbon fluxes between the pelagic and the sediment at $54^{\circ} 5' \text{N}$,
450 8°E in 2011 for a) the "plate run" and b) the reference run. The time in the year when half of the
451 deposited particulate material is returned as DIC is indicated by the black arrow on the x-axis.



452 **9. References**

453 Arakawa, A., and Lamb, V., 1977. "Computational design of the basic dynamical processes of
454 the UCLA general circulation model," in *General Circulation Models of the Atmosphere*, 17,
455 *Methods in Computational Physics: Advances in Research and Applications*, ed. J. Chang
456 (London: Elsevier), 173-265.

457 Backhaus, J., 1985 . A three-dimensional model for the simulation of shelf sea dynamics. *Ocean*
458 *Dynam.*, 38, 165-187. doi: 10.1007/BF02328975.

459 Bozec, Y., Thomas, H., Schiettecatte, L.-S., Borges, A.V., Elkalay, K., De Baar, H.J.W., 2006.
460 Assessment of processes controlling seasonal variations of dissolved inorganic carbon in the
461 North Sea. *Limnol. Oceanogr.*, 51(6), 2746–2762.

462 Brenner, H., Braeckman, U., Le Guitton, M., Meysman, F. J. R., 2016. The impact of sedimentary
463 alkalinity release on the water column CO₂ system in the North Sea. *Biogeosciences*, 13, 841–
464 863.

465 Burdige, D.J. and Komada, T., 2013. Using ammonium pore water profiles to assess stoichiometry
466 of deep remineralization processes in methanogenic continental margin sediments. *Geochemistry,*
467 *Geophysics, Geosystems*, 14(5), 1626–1643.

468 Burt, W.J., Thomas, Pätsch, J., Omar, A.M., Schrum, C., Daewel, I., Brenner, H., de Baar,
469 H.J.W., 2014. Radium isotopes as tracer of sediment-water column exchange in the North Sea.
470 *Glob Biogeo. Cycl.*, 28, 786–804.

471 Große, F., Greenwood, N., Kreuz, M., Lenhart, H. J., Machoczek, D., Pätsch, J., Salt, L. A.,
472 Thomas, H., 2016. Looking beyond stratification: a model-based analysis of the biological drivers
473 of oxygen depletion in the North Sea. *Biogeosciences*, 13, 2511–2535.

474 Gypens, N., Lancelot, C., Soetaert, K., 2008. Simple parameterisations for describing N and P
475 diagenetic processes: Application in the North Sea. *Progr. Oceanogr.*, 76, 89–110.

476 Heinze, C., Maier-Reimer, E., Winguth, A.M.E., Archer, D., 1999. A global oceanic sediment
477 model for long-term climate studies. *Glob. Biogeochem. Cycles*, 13, 221–250.

478 Kalnay, E., Kanamitsu, M., Kistler, R., Collins, W., Deaven, D., Gandin, L., Iredell, M., Saha,
479 S., White, G., Woollen, J., 1996. The ncep/ncar 40-year reanalysis project. *Bulletin of the*
480 *American Meteorological Society* 77 (3), 437–471.

481 Lorkowski, I., Pätsch, J., Moll, A. and Kühn, W., 2012. Interannual variability of car-
482 bon fluxes in the North Sea from 1970 to 2006 – Competing effects of abiotic and biotic



- 483 drivers on the gas exchange of CO₂. *Estuarine, Coastal and Shelf Science*, 100, 38–57, doi:
484 10.1016/j.ecss.2011.11.037.
- 485 Luff, R. and Moll, A., 2004. Seasonal dynamics of the North Sea sediment using a three-dimensional
486 coupled sediment-water model system. *Continental Shelf Research*, 24, 1099–1127.
- 487 Neubacher, E.C., Parker, R.E., Trimmer, M., 2011. Short-term hypoxia alters the balance of the
488 nitrogen cycle in coastal sediments. *Limnology and Oceanography*, 56(2), 651–665.
- 489 Neumann, A., van Beusekom, J. E. E., Holtappels, M., Emeis, K. C. 2017. Nitrate con-
490 sumption in sediments of the German Bight (North Sea) , *Journal of Sea Research*. Doi:
491 10.1016/j.seares.2017.06.012.
- 492 Pätsch, J., Burchard, H., Dieterich, C., Gräwe, U., Gröger, M., Mathis, M., Kapitza, H., Bersch,
493 M., Moll, A., Pohlmann, T., Su, J., Ho-Hagemann, H.T.M., Schulz, A., Elizalde, A., Eden,
494 C., 2017 An evaluation of the North Sea circulation in global and regional models relevant for
495 ecosystem simulations. *Ocean Modelling*, 116, 75–90.
- 496 Pätsch, J., Lenhart, H.-J., Schütt, M., 2016. Daily Loads of Nutrients, Total Alkalinity, Dissolved
497 Inorganic Carbon and Dissolved Organic Carbon of the European Continental Rivers for the
498 Years 1977–2014. Technical Report, Institut für Meereskunde, Universität. Hamburg.
- 499 Pätsch, J., Serna, A., Dähnke, K., Schlarbaum, T., Johannsen, A., Emeis, K., 2010. Nitrogen
500 cycling in the German Bight (SE North Sea) - Clues from modelling stable nitrogen isotopes.
501 *Continental Shelf Research*, 30, 203–213.
- 502 Pätsch, J. and Kühn, W., 2008. Nitrogen and carbon cycling in the North Sea and exchange
503 with the North Atlantic - a model study, Part I. Nitrogen budget and fluxes. *Continental Shelf
504 Research*, 28, 767–787.
- 505 Pangaea, 2017. <https://doi.pangaea.de/10.1594/PANGAEA.872715>
- 506 Paulmier, A., Kriest, I., Oschlies, A., 2009. Stoichiometries of remineralisation and denitrification
507 in global biogeochemical ocean models. *Biogeosciences*, 6, 923–935.
- 508 Pohlmann, T., 1996. Predicting the thermocline in a circulation model of the North Sea .1. Model
509 description, calibration and verification. *Cont. Shelf Res.* 16 (2), 131–146.
- 510 Radach, G. and Pätsch, J., 2007. Variability of Continental Riverine Freshwater and Nutrient
511 Inputs into the North Sea for the Years 1977–2000 and Its Consequences for the Assessment of
512 Eutrophication, *Estuaries and Coast*, 30(1), 66–81.



- 513 Ridgwell A., Zondervan I., Hargreaves J. C., Bijma J., Lenton T. M., 2007. Assessing the potential
514 long-term increase of fossil fuel CO₂ uptake due to CO₂-calcification feedback. *Biogeosciences*
515 4, 481–492.
- 516 Schöpp, W., Posch, M., Mylona, S., Johansson, M., 2003. Long-term development of acid depo-
517 sition (1880-2030) in sensitive freshwater regions in Europe. *Hydrol. and Earth Syst. Sci.*, 7,
518 436–446.
- 519 Seitzinger, S. and Giblin, A.E., 1996. Estimating denitrification in North Atlantic continental shelf
520 sediments. *Biogeochemistry*, 35, 235–260.
- 521 Serna, A., Pätsch, J., Dähnke, K., Wiesner, M. G., Hass, H. C., Zeiler, M., Hebbeln, D., Emeis,
522 K.-C., 2010. History of anthropogenic nitrogen input to the German Bight/SE North Sea as
523 reflected by nitrogen isotopes in surface sediments, sediment cores and hindcast models. *Cont.*
524 *Shelf Res.* 30, 1626–1638.
- 525 Schwichtenberg, F., 2013. Drivers of the carbonate system variability in the southern North Sea:
526 River input, anaerobic alkalinity generation in the Wadden Sea and internal processes, (Dok-
527 torarbeit/PhS), Universität Hamburg, Hamburg, Germany, 161 pp.
- 528 Thomas, H., Sciettecatte, L.-S., Suykens, K., Kone, Y.J.M., Shadwick, E.H., Prowe, A.E.F., Bozec,
529 Y., de Baar, H.J.W., Borges, A.V., 2009. Enhanced open ocean storage from anaerobic alkalinity
530 generation in coastal sediments. *Biogeosciences*, 5, 267–274.

531 **10. Appendix**532 *10.1. Equations for solid and dissolved sediment components*533 Dissolved Matter: exchange with the pelagic ecosystem model ECOHAM

534 ($DIC(i = 1)$, $TA(i = 2)$, $PO_4(i = 3)$, $NO_3(i = 4)$, $NH_4(i = 5)$, $N_2(i = 6)$, $SiO_4(i = 7)$,
 535 $O_2(i = 8)$)

$$\frac{\partial C_i}{\partial t} = dv_i \frac{\partial^2 C_i}{\partial x^2} + \frac{R_j}{P} \quad j = 1, \dots, 6 \quad (5)$$

536 R_j : [$mmol\ m^{-3}\ s^{-1}$] are reaction terms for the dissolved matter. P: Porosity537 dv_i are the vertical diffusion coefficients described in section 2.3.6.538 Solids: input from the pelagic ecosystem model ECOHAM539 ($POM(C/N/P)$, $CaCO_3$, SiO_2 (Opal), Silt (with predefined constant input))

$$\frac{\partial S_j}{\partial t} = D \frac{\partial(w S_j)}{\partial z} - \frac{R_j}{1-P} \quad j = 1, \dots, 5 \quad (6)$$

540 w : vertical advection (downward) R_j : [$mmol\ m^{-3}\ s^{-1}$]541 *10.2. Reaction Terms R_j* 542 • *Degradation of POM*

543 – aerobic degradation (j=1)

$$R_{POC}^{AD} = r_1 \cdot T_{fac}(T) \cdot [POC] \cdot [O_2] \quad (7)$$

544 r_1 : [$\frac{m^3}{mmol\ O_2 \cdot s}$]

545 $R_{PON}^{AD} = R_{POC}^{AD} \cdot \frac{r_{nit}}{r_{car}}$

546 $R_{POP}^{AD} = R_{POC}^{AD} \cdot \frac{1}{r_{car}}$

547 – anaerobic degradation

548 * DNR (denitrification) (j=2)

$$R_{POC}^{DNR} = r_2 \cdot T_{fac}(T) \cdot \left(1 - \frac{[O_2]}{[O_2^{half}] + [O_2]}\right) \cdot \min\left(\frac{1}{2}[NO_3^-]; [POC]\right) \quad (8)$$

549 r_2 : [$\frac{1}{s}$]



550 * SR (sulfate reduction) (j=3)

$$R_{POCs}^{SR} = r_3 \cdot T_{fac}(T) \cdot \min\left(\frac{[TA]}{r_{nit}}; [POC]\right) \quad (9)$$

551 $r_3 : \left[\frac{1}{s}\right]$

552 • *CaCO₃ dissolution* (j = 4)

$$R_{CaCO_3} = r_4 \cdot T_{fac}(T) \cdot [CaCO_3] \cdot (\max([CO_3^{2-}]^{sat} - [CO_3^{2-}]; 0)) \quad (10)$$

553 $r_4 : \left[\frac{m^3}{mmol CO_3^{2-} \cdot s}\right]$

554 $[CO_3^{2-}]^{sat} = \frac{k_{sp}}{Ca}$

555 ksp: apparent pressure corrected solubility product of calcite

556 Ca = 10.3 [mol m⁻³]: Calcium concentration

557

558 • *SiO₂ (Opal Dissolution)* (j=5)

$$R_{SiO_2} = [SiO_2] \cdot r_5 \cdot T_{fac}(T) \cdot ([Si(OH)_4]^{sat} - [Si(OH)_4]) \quad (11)$$

559 $r_5 : \left[\frac{m^3}{mmol Si(OH)_4 \cdot s}\right]$

560 $[Si(OH)_4]^{sat} = 1 \text{ mol m}^{-3}$

561 • *NH₄ (Nitrification)* (j=6)

$$R_{NH_4}^{NO_3} = r_6 \cdot T_{fac}(T) \cdot [NH_4] \quad (12)$$

562 $r_6 : \left[\frac{1}{s}\right]$

$$\text{with } T_{fac}(T) = 1.2^{\frac{T-T_0}{10}} \text{ with } T_0 = 10^\circ C \quad (13)$$



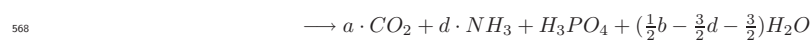
563 10.3. Reaction Equations and Stoichiometry

564 All stoichiometric factors are based on $R_0 = rcar + \frac{1}{4}z$ with $rcar = C/P$

565 and z: H-excess for the notation of organic matter: $C_x (H_2O)_w (NH_3)_y H_z H_3PO_4$

566 1) Incomplete Aerobic Remineralisation (after Paulmier et al., 2009)

567
$$C_a H_b O_c N_d P + \underbrace{\left(a + \frac{1}{4}b - \frac{1}{2}c - \frac{3}{4}d + \frac{5}{4}\right)}_{=ro2ut} \cdot O_2$$



569 with $R_0 = a + \frac{1}{4}b - \frac{1}{2}c - \frac{3}{4}d + \frac{5}{4} \Rightarrow ro2ut = R_0$

570 with $a = rcar = C/P$

571 $b = \quad = H/P$

572 $c = \quad = O/P$

573 $d = rnit = N/P$



574 2) Complete Denitrification (after Paulmier et al., 2009)

$$575 \quad C_a H_b O_c N_d P + \underbrace{\left(\frac{4}{5}a + \frac{1}{5}b - \frac{2}{5}c + 1\right)}_{=nitdem} \cdot HNO_3$$

$$576 \quad \longrightarrow a \cdot CO_2 + H_3PO_4 + \left(\frac{2}{5}a + \frac{3}{5}b - \frac{1}{5}c - 1\right) \cdot H_2O + \underbrace{\left(\frac{2}{5}a + \frac{1}{10}b - \frac{1}{5}c + \frac{1}{2}d + \frac{1}{2}\right)}_{n2prod} \cdot N_2$$

$$577 \quad \text{with } R_0 = a + \frac{1}{4}b - \frac{1}{2}c + \frac{5}{4} \Rightarrow n2prod = \frac{2}{5}R_0 + \frac{4}{5}d = \frac{1}{2}(nitdem + d)$$

$$578 \quad nitdem = \frac{4}{5}R_0 + \frac{3}{5}d$$

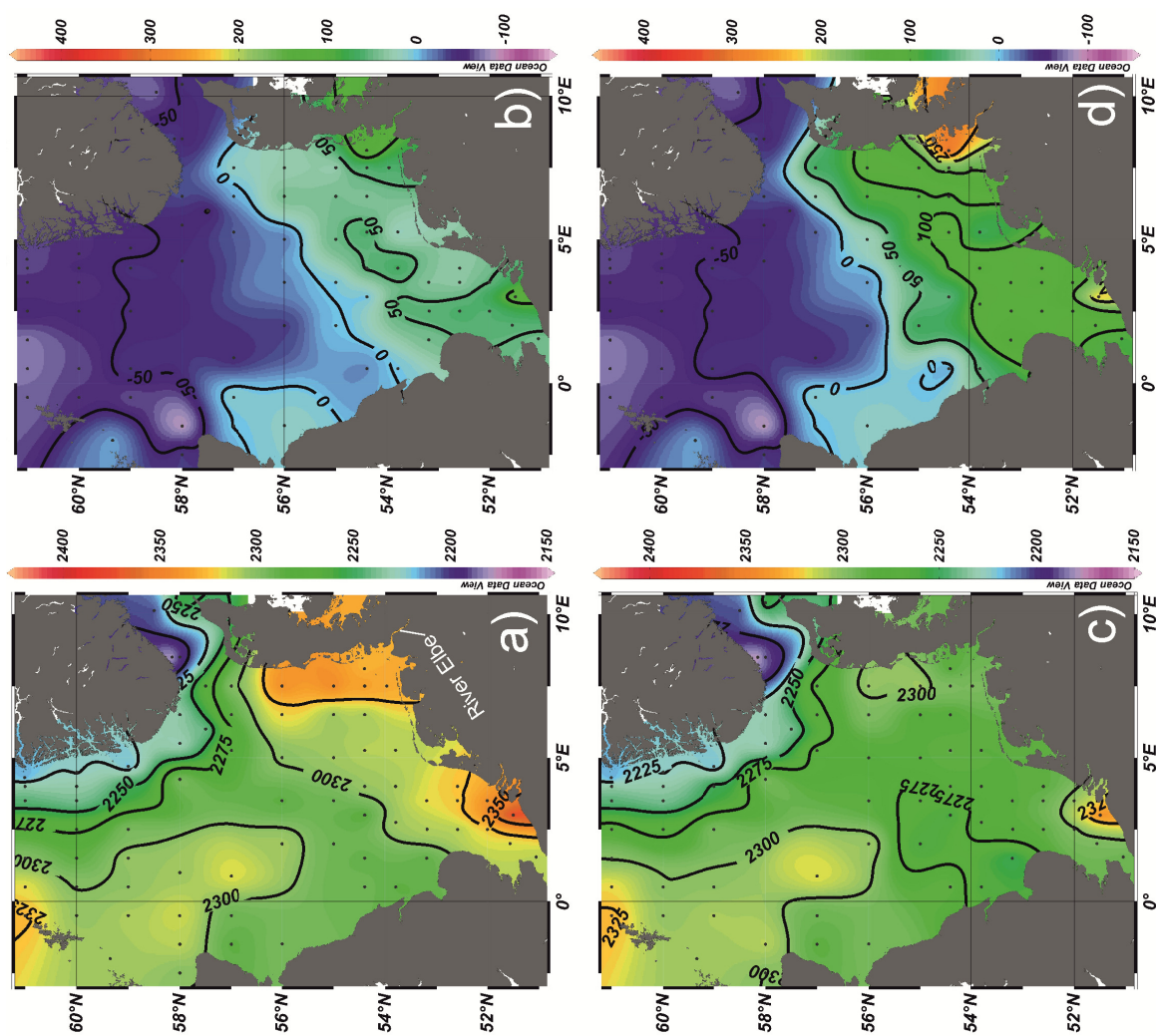


Fig. 1

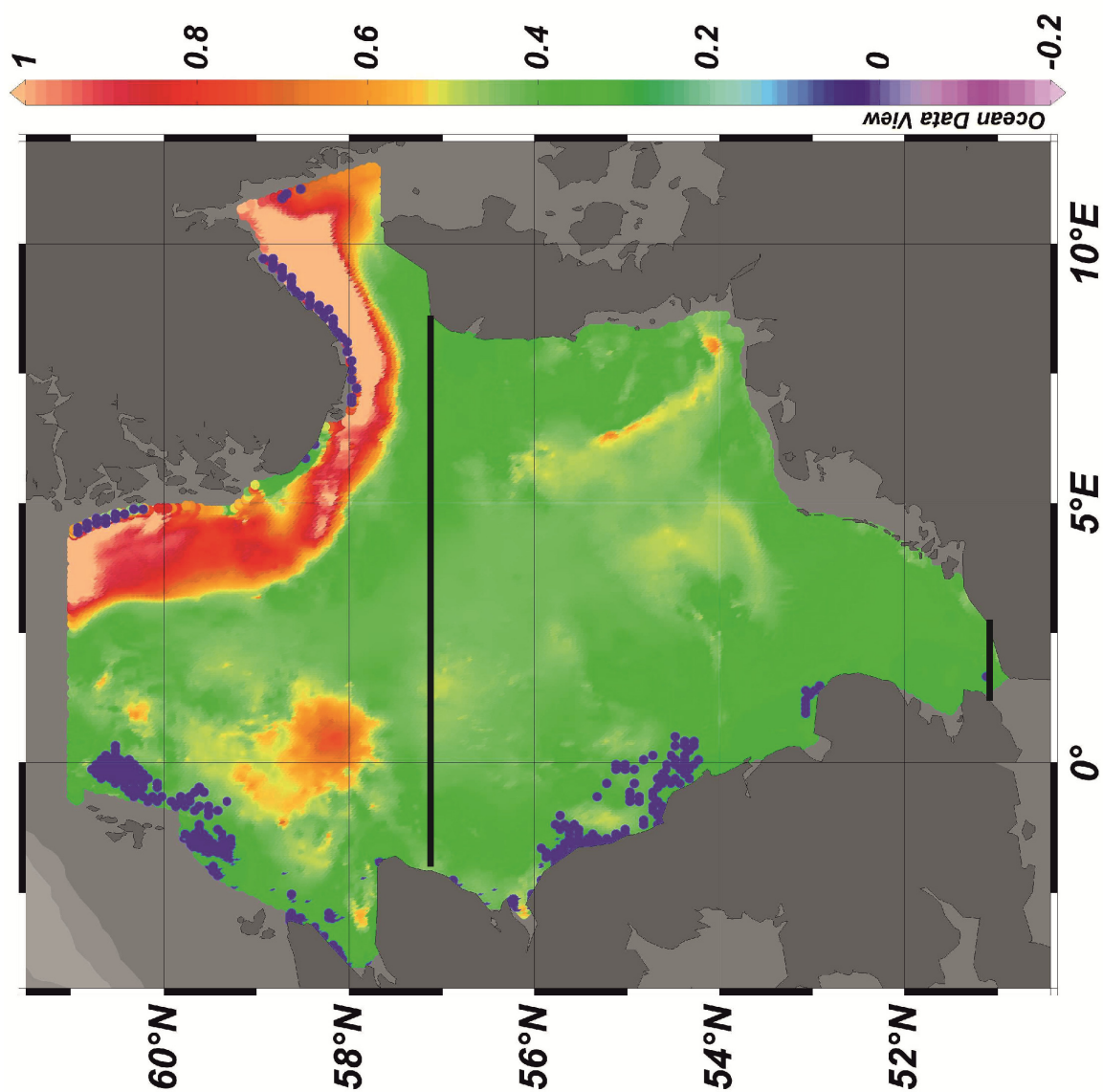


Fig. 2



Fig. 3

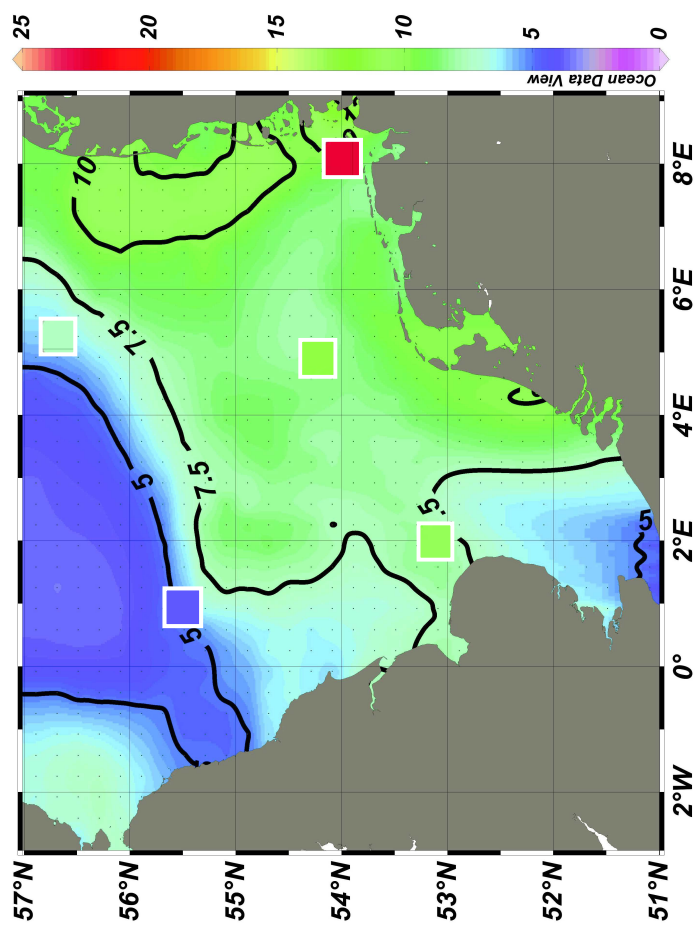
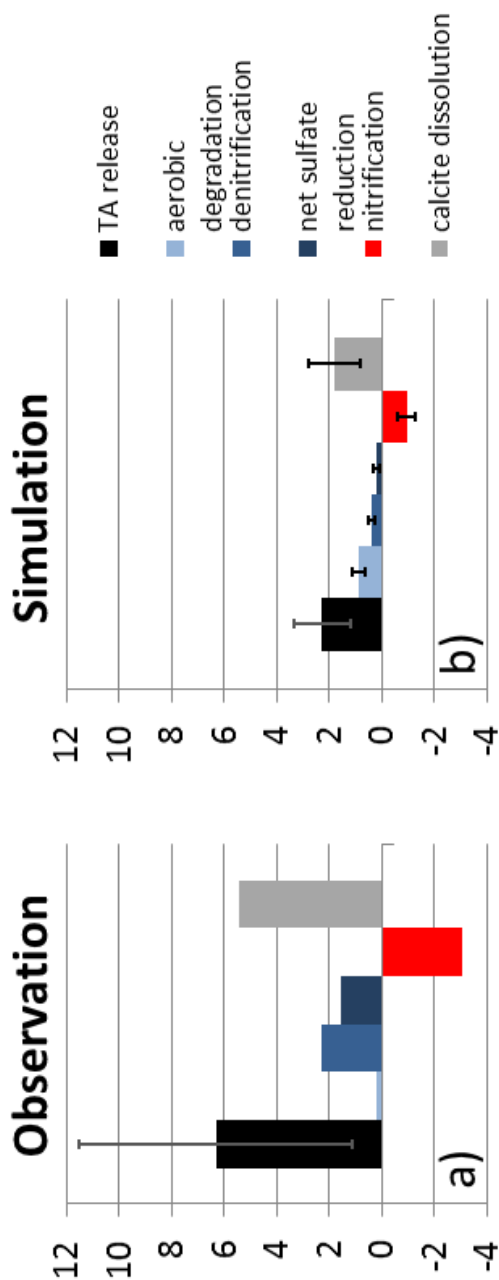




Fig. 4



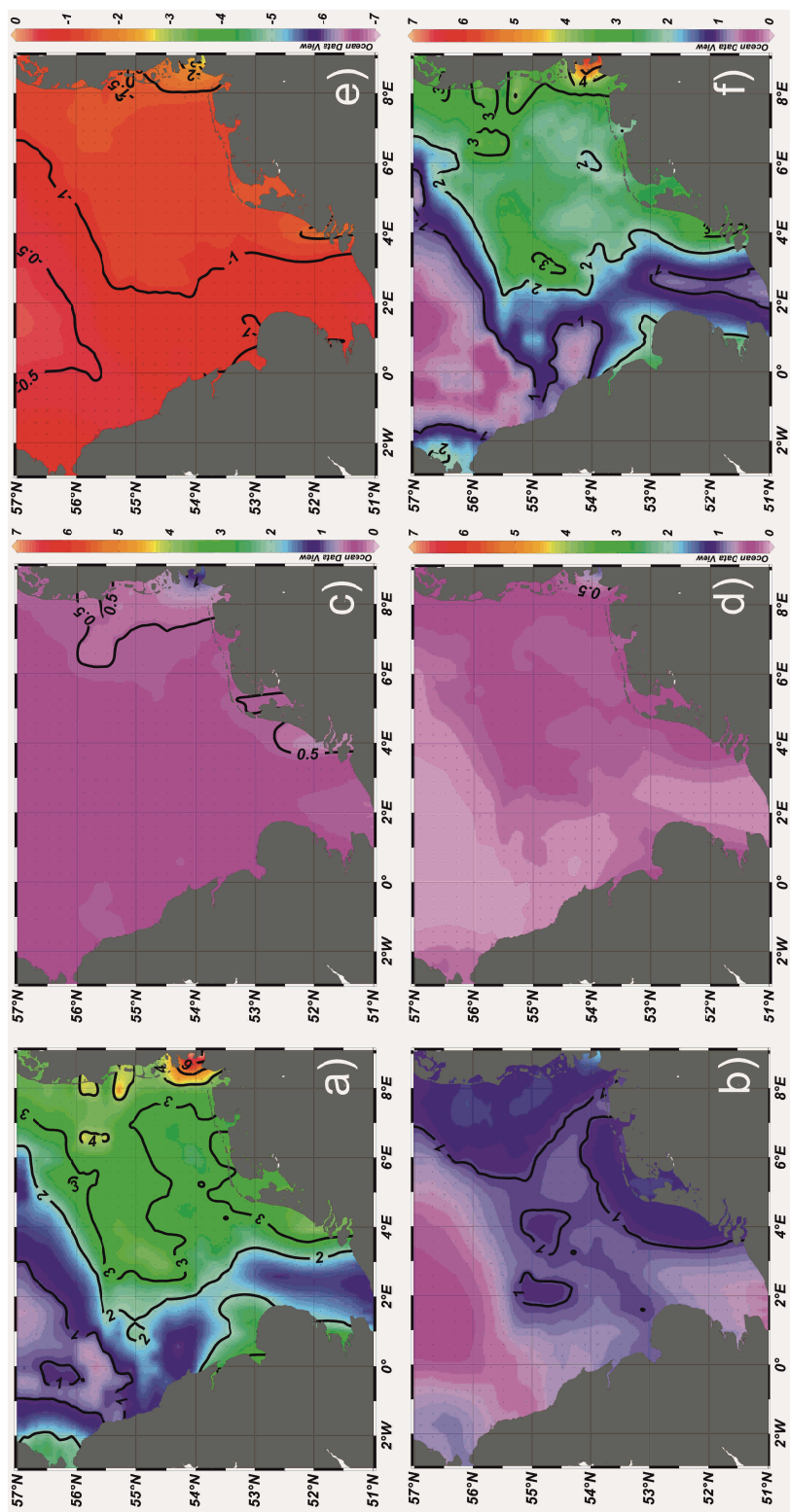


Fig. 5

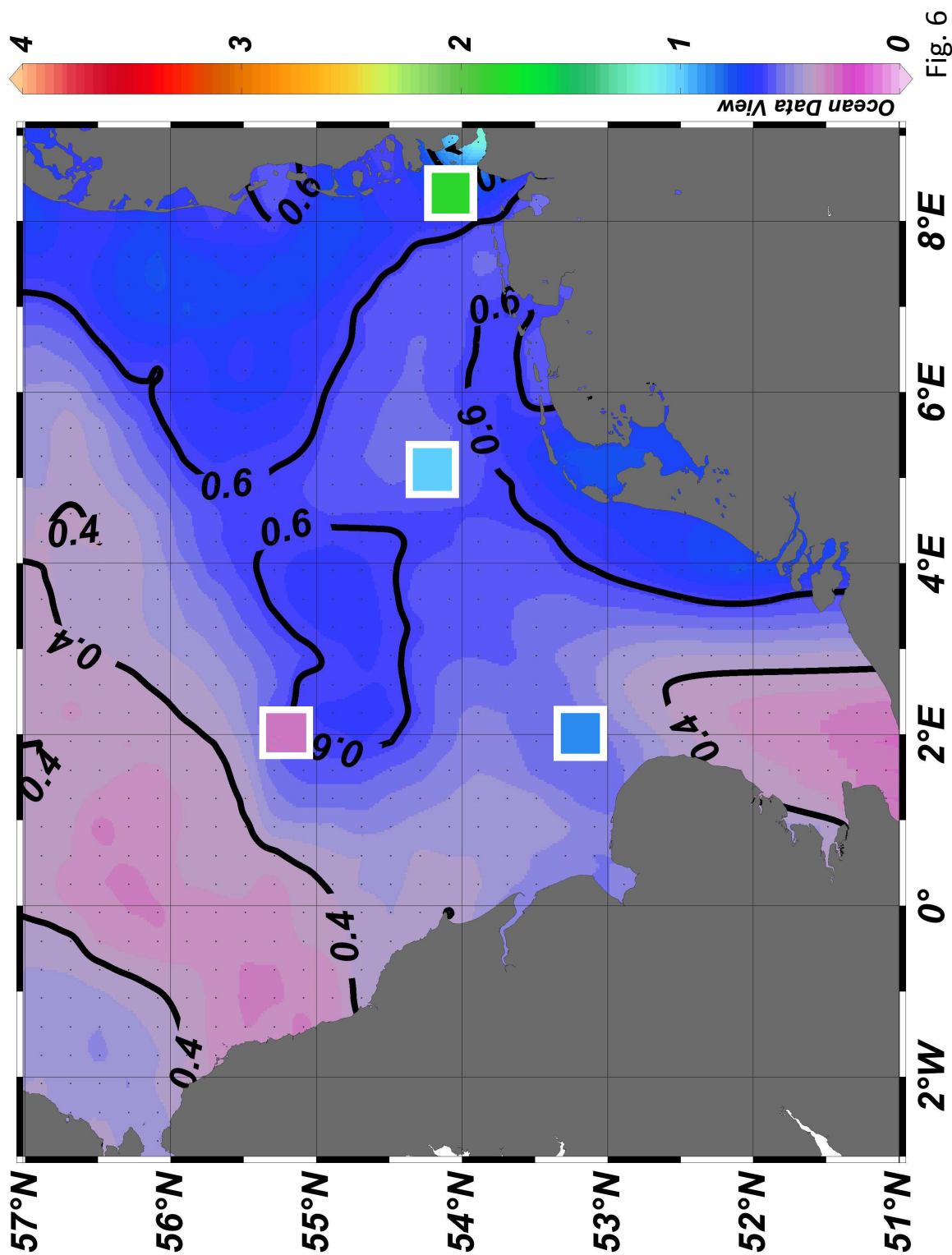


Fig. 6

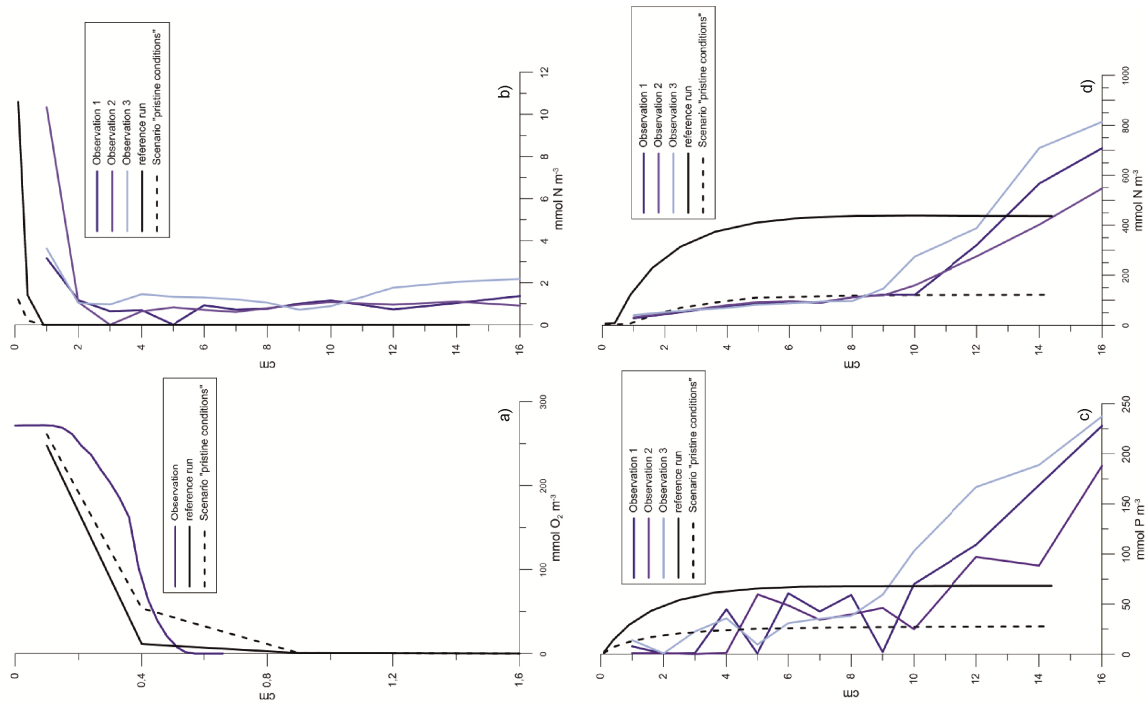


Fig. 7

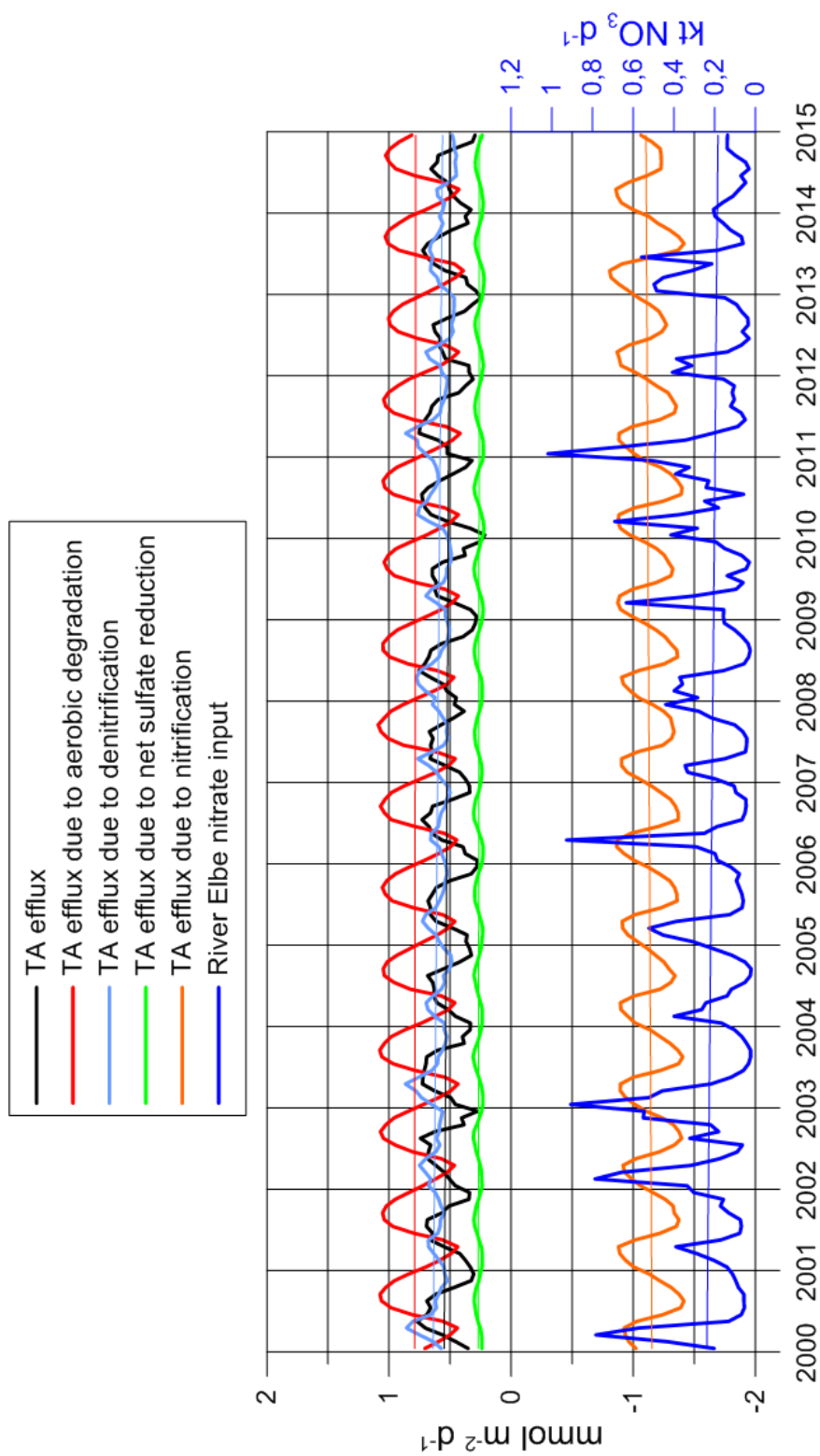


Fig. 8

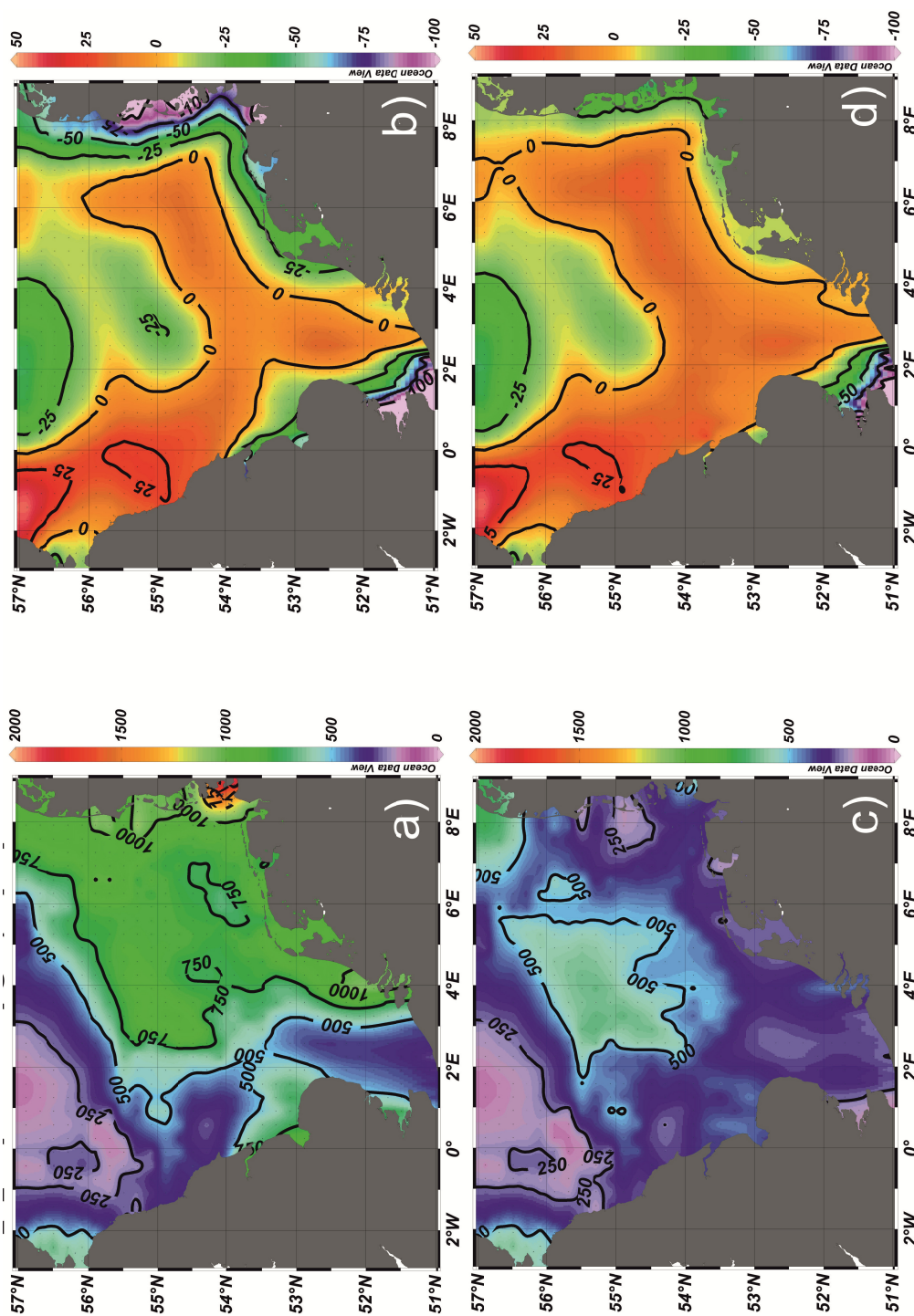


Fig. 9



Fig. 10

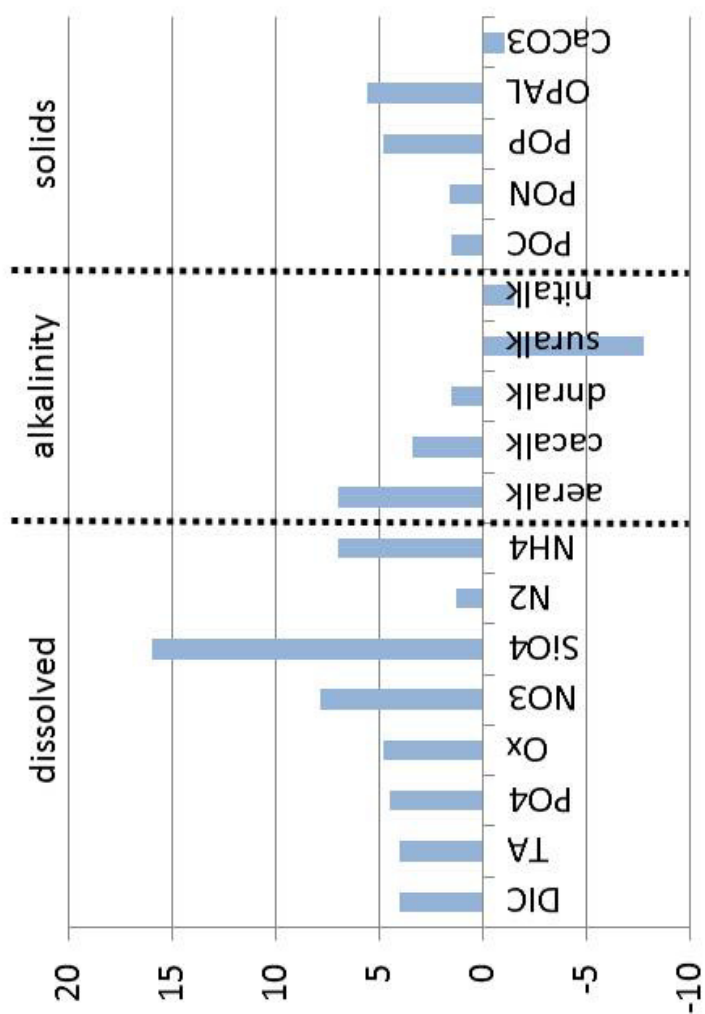




Fig. 11

